이 학 석 사 학 위 논 문

Relative Contribution of Different Plant Functional Types to Growing Season Gross Primary Productivity Interannual Variation in Alaska

식생유형이 알라스카 총 1차 생산성의 연간변화에 미치는 상대적인 기여

February 2018

서울대학교 대학원

협동과정 농림기상학

Jane Lee

RELATIVE CONTRIBTUION OF DIFFERENT PLANT FUNCTIONAL TYPES TO GROWING SEASON GROSS PRAIMARY PRODUCTIVITY INTERANNUAL VARIATION IN ALASKA

UNDER THE SUPERVISION OF
PROFESSOR YOUNGYREL RYU

SUBMITTED TO THE FACULTY OF THE GRADUATE SCHOOL
OF SEOUL NATIONAL UNIVERSITY

BY
JANE LEE

INTERDISCIPLINARY PROGRAM IN
AGRICULTURAL AND FOREST METEOROLOGY

DECEMBER 2017

APPROVED AS A QUALIFIED THESIS OF
JANE LEE

FOR THE DEGREE OF MASTER OF SCIENCE
IN AGRICULTURAL AND FOREST METEOROLOGY
BY COMMITTEE MEMBERS

JANUARY 2018

CHAIRMAN _____
Hyun Seok Kim, Ph.D.

VICE-CHAIRMAN _____
Youngyrel Ryu, Ph.D.

MEMBER _____
Sang Jong Park, Ph.D.

ABSTRACT

Relative Contribution of Different Plant Functional Types to Growing Season Gross Primary Productivity Interannual Variation in Alaska

Jane Lee

Interdisciplinary Program in Agricultural and Forest Meteorology

The Graduate School of Seoul National University

Vegetation in the high latitude ecosystem is most responsive to climate variables, leading to high year to year variability of gross primary productivity (GPP). Therefore, understanding the spatiotemporal patterns of GPP and how climate variables drive its interannual variability (IAV) is important to account for their present and future status. In this study, we examine the spatiotemporal patterns of Alaskan GPP and further investigate how their relation to climate drivers. We use GPP derived from four different approaches, a process-based approach (Breathing Earth System Simulator), a semi-empirical approach (Moderate Resolution Spectroradiometer 17A2) and the machine-learning approaches (Support Vector Regression and FLUXCOM). Model evaluation with eddy covariance data from 17 sites showed that the models explained 65% to 85% of the monthly variation with relative bias ranging from -22% to 33%. Model performance was better in the boreal forest compared to tundra and fire disturbed ecosystems. The spatial and temporal variation of GPP in the models displayed a consistent pattern, where the deciduous broadleaf forest showed the highest variability of GPP IAV by 14%, followed by fire and evergreen forest (13%) and then tundra (10%). Tundra accounted for the largest fraction of IAV of GPP with 55%, exceeding evergreen needleleaf forest (38%), deciduous broadleaf forest (7%) and areas that had been disturbed by fire (0.8%). GPP in tundra has the smallest variation among the PFTs. 68% of Alaska is tundra which led to the largest contribution to the IAV of GPP. The IAV of GPP from 2001 to 2011 had a similar pattern to the IAV of both air temperature and radiation, where warmer years had a larger GPP anomaly compared to the colder years. Therefore, warming and cooling as a result of climate change could significantly impact the IAV of land-atmosphere interaction of carbon dioxide.

Keywords: interannual variation, gross primary productivity, air temperature, radiation, precipitation, Alaska

Student Number: 2015-23147.

TABLE OF CONTENTS

ABSTRACT.....i
TABLE OF CONTENTS..... ii
LIST OF TABLE iii
LIST OF FIGURES iv
1. Introduction.....5
2. Material and Method.....9
2.1 Study Region 9
2.2 Flux Tower Data..... 10
2.3 Satellite-based GPP Datasets 13
2.4 Dataset of climate variables 18
2.5 Landcover map.....19
2.6 Evaluation and analysis of GPP 20
3. Results.....24
3.1 Evaluation of Models against flux tower data..... 24
3.2 IAV of GPP 27
3.3 Relationship between IAV of GPP and Climate Variables..... 35
4. Discussion.....41
4.1 Model Performance across different PFTs 41
4.2 IAV of GPP 43
4.3 Controlling factors in IAV of GPP..... 45
5. Conclusion 47
References.....48

Abstract in Korean 57
Acknowledgement 58

LIST OF TABLE

Table 1. Flux tower site information.....11
Table 2. Summary of Model Approach and MODIS input forcing data.....17
Table 3. Evaluation of BESS, MODIS, SVR and FLXUCOM……24

LIST OF FIGURES

Figure 1 Plant functional type map of Alaska.....10

Figure 2 Evaluation of modeled GPP at a monthly time scale. 27

Figure 3 The Relative standard deviation (%) of GPP IAV 29

Figure 4 Averaged relative standard deviation of GPP IAV. 30

Figure 5 Relative contribution (%) of each grid cell to GPP IAV. 32

Figure 6 (a) The sum of relative contribution of GPP IAV for each PFT, and the (b) the IAV of GPP from 2001 to 2011 in Alaska. 33

Figure 7 Relative contribution of PFT to GPP 35

Figure 8 RGB composite of climatic drivers. 37

Figure 9 The mean and sum of relative contribution to GPP IAV. 39

Figure 10 The IAV pattern of GPP. 45

1. Introduction

The Arctic ecosystem, characterized by low temperatures and short growing seasons, plays a unique role in the land-atmosphere exchange of carbon dioxide (Bliss *et al.,* 1973, McGuire *et al.,* 2006, Schuur *et al.,* 2015). During the Holocene (approximately 11,700 years ago), the arctic system was a net carbon sink (Oechel *et al.,* 1993, Ping *et al.,* 2008), with pervasive cold temperatures limiting the decay of soil organic carbon, resulting in the accumulation of carbon above and beneath the permafrost in peatlands over centuries to a millennia (Strauss *et al.,* 2013). Substantial warming, induced by anthropogenic fossil fuel emission, in the high latitudes is occurring faster compared to the rest of the globe (Bekryaev *et al.,* 2010, Bieniek and Walsh 2017). This is causing frozen ground to thaw, exposing large quantities of organic carbon to soil microbes for decomposition, leading to the release of greenhouse gases into the atmosphere that could increase the rate of global warming (Nauta *et al.,* 2014, Schuur *et al.,* 2015). Warming is also lengthening growing seasons allowing vegetation productivity to increase (Jeong *et al.,* 2011, Guay *et al.,* 2014, Park *et al.,* 2016), or stimulating respiration depending on plant functional types (Piao *et al.,* 2008, Euskirchen *et al.,* 2016, Commane *et al.,* 2017), affecting the carbon balance of the ecosystem. Such changes in the arctic ecosystem may further amplify or dampen feedbacks to climate change (ChapinIII

et al., 2005, Zeng *et al.,* 2017).

Changes in gross primary productivity (GPP) across different plant functional types (PFT) are non-linear in the high latitudes as they are affected by warming in the recent decades (Park *et al.,* 2015). GPP in the cooler high latitudes show an increase, due to warming, while the warmer lower latitudes show a decline (Mekonnen *et al.,* 2016). Ueyama *et al.,* (2014) reveals that a black spruce forest in the Interior of Alaska shifted from a CO_2 sink to source as autumn air temperatures increased over 9 years. Satellite observations also show that the boreal forests are "browning" whereas arctic tundra continues "greening." (Beck and Goetz 2012, Xu *et al.,* 2013). The response of vegetation to climate drivers can change (Piao *et al.,* 2014, Wang *et al.,* 2015, Piao *et al.,* 2017), therefore, it is important to understand the spatiotemporal patterns of GPP and how climate variables drive its year to year variability to account for their present and future status.

The pattern of GPP interannual variability (IAV) is determined by climate variables, vegetation types and their spatial distribution (Zhang *et al.,* 2016, Zhou *et al.,* 2017). GPP in tundra ecosystems is controlled by environmental factors such as, the time of snowfall or snowmelt and leaf out and leaf fall, which determines growing season length (Euskirchen *et al.,* 2012, Ueyama *et al.,* 2013). In evergreen needleleaf forests (ENF), GPP is detected when the environment becomes favorable as their photosynthetic apparatus are already assembled (Goulden *et al.,* 1998, Welp

et al., 2007). GPP in deciduous broadleaf forests (DBF) are more sensitive to spring temperatures and lags compared to ENF as leaf develops, but after leaf-out they compensate for the late start by higher assimilation rates during the middle of the growing season (Black *et al.,* 2000, McGuire *et al.,* 2006, Welp *et al.,* 2007, Zhang *et al.,* 2017). Forests disturbed by fire have smaller GPP than undisturbed forests, but with varying magnitude of GPP depending on the rate of recovery, which increases the rate of carbon dioxide IAV in the northern hemisphere (Randerson *et al.,* 2006, Yi *et al.,* 2013). In short, the larger variation of GPP in ENF is modulated by physiology rather than phenology. In contrast, both the physiology and phenology of DBF, tundra and disturbed sites explains GPP IAV. Previous studies have intensively focused on how the structure of canopy, leaf-on and leaf-fall of different PFTs affect GPP responses to climate variability (Yuan *et al.,* 2009, Mekonnen *et al.,* 2016), but we still lack a comprehensive understanding of how different PFTs contribute to GPP IAV in Alaska.

Gross primary productivity can be derived from a regional to global scale through combining various approaches, such as the process-based, semi-empirical or machine learning, with remote sensing products and meteorological datasets. Process-based approaches employ biophysical theories to provide insight to the underlying mechanisms of environmental change on vegetation activity (Ryu *et al.,* 2011, Jiang and Ryu 2016). Semi-empirical approaches use algorithms with

empirical constraints to estimate the desired variable such as light use efficiency (Running *et al.,* 2004). Machine-learning approaches use exiting data to train statistical models, and apply the model to a larger area with the explorative variables (Ueyama *et al.,* 2013, Tramontana *et al.,* 2016). Major model comparison projects demonstrate that there are large variations within model estimations of GPP due to varying forcing data, model structure and parameterization, yet an ensemble of models can reduce bias of estimates from models (Cramer *et al.,* 1999, Sitch *et al.,* 2007, Huntzinger *et al.,* 2013, Piao *et al.,* 2013, Ito *et al.,* 2016). Therefore, we use the products of these different approaches to analyze the spatial and temporal patterns of GPP interannual variability and its response to with climate variability.

Here, our goal is to quantify the spatial and temporal patterns of GPP IAV in Alaska growing season. To achieve our goal, we test the performance of four GPP models against 17 flux tower data from different PFTs. Then we investigate the spatial and temporal patterns of GPP, quantifying the relative contributions of PFTs to GPP IAV in Alaska. Finally, we examine the relationship of GPP with climate variables at a regional scale.

2. Material and Method

2.1 Study Region

We defined our study region, Alaska, excluding the southeastern Alaskan Panhandle, with latitudes and longitudes of 72˚N to 52˚N and 170˚W to 140˚W, respectively. Alaska can be mainly characterized as the Arctic and interior Alaska, based on climate, vegetation type and permafrost distribution. The Arctic is found north of the Brooks Range, covered by tundra vegetation with continuous permafrost. The interior of Alaska is located north of the Alaska Range and south of the Brooks Range, which is mostly boreal forest underlying discontinuous permafrost. The annual mean air temperature is -12˚C and annual precipitation is 100 to 130 mm yr^{-1} in Alaska.

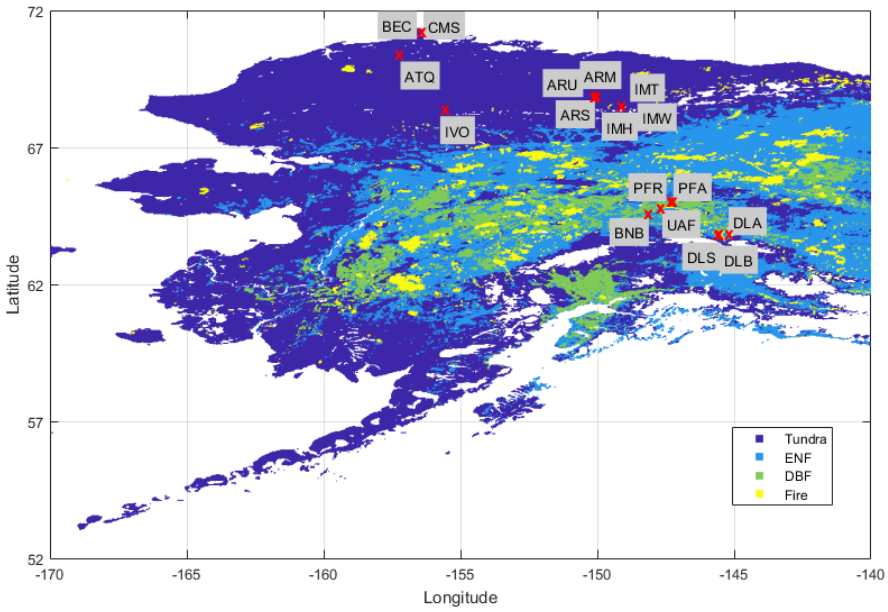

Figure 1 Plant functional type map of Alaska

2.2 Flux Tower Data

Eddy covariance flux data of GPP gathered from 21 sites in Alaska was used in courtesy of Ueyama *et al.,* (2013) for model evaluation. The tower sites are situated in various representative ecosystems of Alaska (Figure 1): wet sedge tundra (CMS, BEC and IMW), moist tussock tundra (ATQ, IVO, IMT and ARU), black spruce forest (PFA, UAF and DLS), Aspen forest (DLA) and burned black spruce forest (CRF, PFR and DLB). The winter and growing season data was present for 13 of the sites, and only the growing season was available for 7 of the sites. Our study period is from 2001 to 2011, where 17 of the 21 sites were available for

evaluating GPP from models. Table 1 presents detailed information of each site.

All data were processed with a standardized gap filling, quality control and flux-partitioning procedures. The quality control of the eddy covariance data was primarily conducted by site mangers. Ueyama *et al.,* (2013) manually removed the outliers and spike-like data and applied a look-up table and nonlinear regression for gap filling and flux partitioning methods. If a lookup table was not applicable, then the nonlinear regression was used. One precaution about partitioning GPP and Ecosystem Respiration (ER) from Net Ecosystem Exchange (NEE) is that nighttime data was used, where nighttime is almost nil in summer. Nighttime data is limited in the Arctic, and thus the performance of respiration models may be less accurate compared to other regions. These flux data were used to upscale from a site level to a regional scale in Alaska with the Support Vector Regression Model from the period of 2000 to 2011 (Ueyama *et al.,* 2013).

Table 1. Flux tower site information

Site Code	Lat (° N)	Lon (° W)	Vegetation Type (PFT)	Years	Mean Annual Temperature[1] (° C)	Mean Annual Precipitation[2] (mm)	Reference
University of Alaska Fairbanks (UAF)	64.87	-147.86	Black Spruce Forest (ENF)	2003-2014	-1.83	309.12	(Iwata *et al.,* 2012); (Ueyama *et al.,* 2014)
Poker Flat Research Range (PFR)	65.12	-147.43	Burned Forest (ENF)	2009-2012	-1.94	308.36	(Iwata *et al.,* 2011)
Poker Flat Research Range (PFA)	65.12	-147.49	Black Spruce Forest (ENF)	2011-2014	-1.94	308.36	(Nakai *et al.,* 2013)
Bonanza Creek LTER (BNB)	64.69	-148.32	Black Spruce Forest (ENF)	2010-2013	-1.94	308.36	(Euskirchen *et al.,* 2012)
Delta Junction (DLS)	63.92	-145.75	Black Spruce Forest (ENF)	2003-2005	-1.67	295.15	(Randerson *et al.,* 2006); (Welp *et al.,* 2007)
Delta Junction (DLA)	63.92	-145.37	Aspen Forest (DBF)	2002-2004	-1.67	295.15	(Randerson *et al.,* 2006); (Welp *et al.,* 2007)
Delta Junction (DLB)	63.89	-145.74	Burned Forest (ENF)	2002-2004	-1.67	295.15	(Randerson *et al.,* 2006); (Welp *et al.,* 2007)
Anaktuvuk River (ARS)	68.98	-150.28	Severely Burned Tundra	2008-2010	-11.00	122.17	(Rocha and Shaver 2011)
Anaktuvuk River (ARM)	68.95	-150.21	Moderately Burned Tundra	2008-2010	-11.00	122.17	(Rocha and Shaver 2011)
Anaktuvuk River (ARU)	68.93	-150.27	Tussock Tundra	2008-2010	-11.00	122.17	(Rocha and Shaver 2011)
Barrow Environmental Observatory (BEC)	71.28	-156.6	Wet Sedge Tundra	2005-2008	-11.22	115.06	(Zona *et al.,* 2011, Zona *et al.,* 2012)
Central	71.31	-156.62	Tundra	1999-	-11.22	115.06	(Harazono *et*

Marsh (CMS)				2005			*al.,* 2003)
Imnavait Creek (IMH)	68.61	-149.3	Heath Tundra	2007-2011	-10.08	247.65	(Euskirchen *et al.,* 2012)
Imnavait Creek (IMW)	68.61	-149.31	Wet Sedge Tundra	2007-2011	-10.08	273.05	(Euskirchen *et al.,* 2012)
Imnavait Creek (IMT)	68.61	-149.3	Moist Acidic Tundra	2007-2011	-10.08	298.45	(Euskirchen *et al.,* 2012)
Atqasuk (ATQ)	70.47	-157.41	Moist Tussock Tundra	1999-2006	-11.22	115.06	(Kwon *et al.,* 2006)
Ivotuk (IVO)	68.49	-155.75	Moist Tussock Tundra	2004-2011	-	-	(Kwon *et al.,* 2006)

2.3 Satellite-based GPP Datasets

To investigate the IAV of GPP in Alaska we used GPP maps from the Breathing Earth System Simulator (BESS), Moderate Imaging Spectroradiometer (MOD17 A), Support Vector Regress (SVR) and FLUXCOM from a period between 2001 to 2011 in Alaska. We use GPP from these from different approaches (process-based, semi-empirical and machine-learning) as major model comparison projects show that an ensemble of models can reduce bias of estimates from models. A summary of the model structure and forcing data is shown in **Table 2**.

[1] Available at the Western Regional Climate Center, NCDC (National Climatic Data Center) 1981 – 2010 normals

[2] Available at the Western Regional Climate Center, NCDC (National Climatic Data Center) 1981 – 2010 normals

We used BESS data from Jiang and Ryu (2016), which are also publically available at http://environmenta.snu.ac.kr/. BESS is a concise biophysical model that computes GPP and ET at 8-day temporal and 1km spatial resolution using remote sensing data from 2000 to 2015. BESS computes direct and diffuse radiation in the photosynthetically active radiation (PAR) and near infrared (NIR) spectral domains with an atmospheric radiative transfer model, Forest Light Environmental Simulator (FLiES) (Ryu *et al.,* 2011, Ryu *et al.,* 2018). Then, absorbed PAR and NIR radiation for sunlit and shade canopy is computed by a two-leaf and two-stream canopy radiative transfer model. A PFT dependent look-up table quantifies maximum carboxylation capacity at 25°C ($V_{max}^{25\,C}$), which was further upscaled from a leaf level to a sunlit and shade canopy level (Ryu *et al.,* 2011, Jiang and Ryu 2016). Then a carbon-water-coupled module incorporated a two-leaf longwave radiative transfer model, Farquhar's photosynthesis model, Ball-Berry stomatal conductance equation to compute GPP for sunlit and shade canopy. The instantaneous estimates of GPP were temporally upscaled to 8-day mean estimates using a simple cosine function (Ryu *et al.,* 2012). From the global dataset we extracted Alaska with latitudes from 72˚N to 52˚N and longitudes from 170˚W to 140˚W. The 8 daily data were also converted to monthly data.

We used MOD17A2 GPP (Collection 5.5) products of 8 daily composite with 1km resolutions from a period of 2001 to 2011. MOD17A2 GPP product is built

upon the light use efficiency (LUE) model (Running et al., 2004), assuming that GPP is directly related to absorbed photosynthetically active radiation (APAR) under ideal conditions. A PFT-dependent look-up table is used for maximum LUE, which was downregulated with environmental stress functions in air temperature and water stress. MOD15A2 fPAR product that incorporates atmospherically corrected MODIS surface reflectance and a LUT method to achieve an inversion of the three dimensional radiative transfer process in vegetation canopies is used in deriving MOD17A2 GPP products.

Support vector regression (SVR) based GPP products with temporal and spatial resolution of 8 day composite and 1/30° resolution, respectively, from 2001 to 2011 from Ueyama *et al.,* (2013) were used. SVR is one of the Kernel methods in machine learning that converts nonlinear regressions to linear regressions. The SVR product synthesized 21 site level eddy covariance observations over different plant functional types in Alaska with inputs from satellite products and gridded climate reanalysis dataset (Japanese Re-Analysis 25 years – JRA25) to upscale from a local to regional scale. SVR also classified land areas that had experienced fire in the last ten years because Goulden et al., (2006) demonstrated that EVI and CO_2 uptake during midday became comparable to those at unburned sites. These products were thoroughly tested and were used to investigate the spatial pattern of CO_2 in the growing season in the arctic and boreal ecosystem of Alaska (Ueyama *et al.,* 2013).

GPP were provided in 8 day composite at 1/12° resolution from 2001 to 2011 by Tramontana *et al.,* (2016). FLUXCOM uses an ensemble of 11 machine-learning methods that integrate FLUXNET La Thuile synthesis dataset that had 224 site level observations, satellite remote sensing data and meteorological data. There are 6 FLUXNET sites in Alaska, 3 in the Arctic regions (Atqasuk, Barrow and Ivotuk) and 3 in the boreal regions (Bonzona Creek 1, Bonzona Creek 2 and Bonzona Creek 3). The 11 algorithms from four broad families are: model tree ensembles, multiple adaptive regression splines, artificial neural networks and kernel methods. The tree-based methods are based upon hierarchical binary decision trees (for example, random forest and model tree ensemble). Multivariate regression spline is a non-parametric regression technique that models nonlinearities and interactions between variables. Neural networks use nonlinear and nonparametric regression functions (for example, artificial neural network and group method of data handling). Kernel methods measure the similarity of input data (for example, support vector regression, kernel ridge regression and Gaussian process regression).

Table 2. Summary of Model Approach and MODIS input forcing data

	BESS	MODIS	SVR	FLUXCOM
Type of Approach	Process-based	Semi-empirical	Machine-learning	Machine-learning
Gross Primary Production	Farquhar *et al.,* (1980) PFT-dependent Look-up Table for V_{cmax} [25]	Light Use Efficiency PFT-dependent Look-up Table (MOD172A)	Support Vector Regression from 21 eddy covariance sites	Random Forest, Model Tree Ensemble, Multivariate Regression Splines, Artificial Neural Network, Group Method of Data Handling, Support Vector Regression, Kernel Ridge Regression, Gaussian process regression
Spatial Resolution (°) and Range	1/100° Global	1/100° Global	1/30° Alaska	1/12° Global
Temporal Resolution and Range	8 Day 2000 – 2015	8 Day 2000 – 2015	8 Day 2000 – 2011	8 Day 2001 – 2012
Climate Dataset	NCEP/NCAR Reanalysis ERA-Interim	NCEP/NCAR Reanalysis II	Japanese Reanalysis (JRA25)	ERA-Interim
Radiation Dataset (Spatial Resolution)	BESS Radiation (0.05°)	Global Modeling and Assimilation Office (1° x 1.25 °)	JRA25 (1.1°)	ERA-Interim (0.75°)
MODIS Input Products	Leaf Area Index (MCD 15A2)	Land Surface Temperature (MOD11A1) Leaf Area Index and fPAR (MOD 15A2)		

Other MODIS Input Products	Aerosol (MOD04_L2) Atmosphere Profile (MOD07_L2) Cloud (MOD06_L2) Albedo (MCD43B3) Surface Temperature (MOD11A1)		Surface reflectance - GR (MOD09A2)	NDVI & EVI (MOD13A2) MCD43A2/4 Bidirectional Reflectance Distribution Function
Landcover		Landcover (MCD12A1)	Alaska Geospatial Data Clearinghouse	
Reference	(Ryu *et al.,* 2011, Jiang and Ryu 2016)	(Running *et al.,* 2004, Zhao *et al.,* 2006)	(Ueyama *et al.,* 2013)	(Tramontana *et al.,* 2016)

2.4 Dataset of climate variables

To examine the relationship of GPP with air temperature, precipitation and shortwave radiation, we used gridded climate data. For air temperature and precipitation, we used monthly CRU (Climate Research Unit) TS2.31 Mean Temperature and CRU T323 Precipitation dataset, respectively, which is monthly gridded data based on daily values with a spatial resolution of 0.5° (Harris *et al.,* 2014). This climate dataset is constructed based upon more than 4500 meteorological stations distributed around the world. This data assembles multiple station variables from numerous data sources into a consistent format. Shortwave radiation data was obtained from the Breathing Earth System Simulator (BESS) at

5km, 4 daily spatial temporal resolutions, which was created by merging an atmospheric radiative transfer model with model with an artificial neural network using MODIS atmosphere and land products (Ryu *et al.,* 2018). We used these climate variable data (CRU air temperature, CRU precipitation and BESS shortwave radiation) with latitudes between 71.5°N and 51.5°N and longitudes from -170°W to 140°W in the period during the period between 2001 and 2011. CRU data is available at https://climatedataguide.ucar.edu/climate-data/cru-ts321-gridded-precipitation-and-other-meteorological-variables-1901. BESS shortwave products are publically available at http://environment.snu.ac.kr/ .

2.5 Landcover map

To classify plant functional types (PFTs), we used landcover data from Ueyama *et al.,* (2013), who regrouped data from Alaska Geospatial Data Clearinghouse to represent four PFTs: tundra (68 %), evergreen needleleaf forest (26%), deciduous broadleaf forest (4%) and fire scars (0.9%), hereafter called fire (**Figure 1**). Fire is a new classification in the landcover data which was added as the relationship between CO_2 fluxes and environmental and satellite observations on ecosystems disturbed by fire was substantially different from later successional ecosystems (Randerson *et al.,* 2006, Welp *et al.,* 2007, Ueyama *et al.,* 2013). Fire scars are areas where fire has occurred in the last 10 years based on data from the Alaska Fire

Service. 10 years was used as a proxy to determine the appropriate pixel as fire scar based on research showing that approximately 10 years after a fire event, EVI and CO_2 uptake during midday was comparable to unburned sites.

2.6 Evaluation and analysis of GPP

To evaluate model performance with the 17 flux tower site data, we extracted the pixel that was closest to the tower using Delaunay Triangulation and nearest neighbor. We used a statistical threshold to remove poor daily flux data and then gap filled using a two-dimensional interpolator to conserve the mean diurnal variation. Subsequently, we averaged daily flux data to 8 days, only selecting days that had less than 25% gap filling. In other words, we discarded 8-day composite data where 6 or more days had been gap filled. For monthly variation we averaged the daily to monthly data, again selecting only monthly data where less than 25% of the data had been gap filled.

To test the performance of models in Alaska, we used linear regression, correlation coefficient (r^2), root mean squared error (RMSE), relative RMSE (rRMSE), bias and relative bias (rBias) between the observed values from flux data and predicted values from BESS, MODIS, SVR and FLUXCOM, using the following equations:

$$RMSE = \sqrt{\frac{1}{n}\sum_{i=1}^{n}(X_{obs} - X_{model})^2} \quad \text{(Eq. 1)}$$

$$\textit{Relative RMSE}\ (\%) = (\textit{RMSE} / \overline{X_{obs}}\ ) \times 100 \quad \text{(Eq. 2)}$$

$$Bias = \overline{X_{obs}} - \overline{X_{model}} \quad \text{(Eq. 3)}$$

$$\textit{Relative Bias}\ (\%) = (\textit{Bias} / \overline{X_{obs}}\ ) \times 100 \quad \text{(Eq. 4)}$$

Where, X_{obs} is GPP from flux data, X_{model} is GPP estimated by the model and overbar indicates average.

To investigate the relationship of (IAV) of GPP with climate variables, we aggregated the spatial resolution of BESS (0.01°), MODIS (0.01°), SVR (0.033°) and FLUXCOM (0.083°) to 0.5° grids to compare using the same spatial resolution of climate datasets. The 8 daily composite GPP data were converted to monthly data. We defined growing season as the months when air temperature is above 5°C for each grid cell, assuming that this is when snow has fully melted and leaf has come out so that vegetation may start photosynthesizing (Molau and Molgaard 1996), thus the number of growing season months for each grid cells may be different. We quantified interannual variation and anomaly for just the growing season, as GPP in the winter months is constantly negligible whether winter is relatively warm or

cold.

For all analysis, annual growing season anomaly of GPP, air temperature, precipitation and shortwave radiation were used. Anomaly was calculated as the aberration of the ten year mean of the detrended growing season GPP or climate variable. To investigate the response of GPP IAV with climate variables (air temperature, precipitation and shortwave radiation), we used monthly Z Scores, which are growing season anomalies normalized by its standard deviation.

We used Ahlström *et al.,* (2015)'s method to partition the relative contribution of PFTs to interannual variation of GPP in Alaska. For a given flux (GPP), the contribution of IAV of a grid cell or PFT *j* to the GPP IAV is defined as:

$$fj = \frac{\sum_t \frac{xjt\,|Xt|}{Xt}}{\sum_t Xt} \text{ (Eq. 6)}$$

Where x_{jt} is the flux anomaly for PFT *j* at time *t* (in years) and X_t is the global flux anomaly. X_t is the total flux anomaly, so that $Xt = \sum_j x_{jt}$. We use this method to compare the relative contribution of PFTs in driving global GPP IAV, where PFTs with high scores drive the overall variation, while low scores contribute less with the total sum being equal to 1. Further information of this method can be found in

the supplementary materials of Ahlström *et al.,* (2015).

To examine which PFT governed the IAV of GPP in Alaska, we partitioned GPP IAV quantifying the relative contribution of each grid cell and then summing up for each PFT. The relative contribution can be negative or positive as it quantifies the relative importance to governing GPP IAV, thus the total sum is 1. Then we examined the magnitude of growing season GPP IAVs during 2001 to 2011, with relative standard deviation. To investigate the spatial and temporal drivers of GPP IAV by PFT, we performed a partial correlation analysis between growing season GPP anomalies and climate variables, air temperature, precipitation and shortwave radiation.

3. Results

3.1 Evaluation of Models against flux tower data

Evaluation at the site scale showed that the model performance of BESS, MODIS, SVR and FLUXCOM were substantially different in PFTs. Generally, the four models explained 58% to 82% of the variability in GPP over the different plant functional types (**Figure 2 and Table 3**). Among the 4 different PFTs all models, whether process based or machine learning, performed better in ENF and DBF with high r^2, low RMSE and small bias, compared to tundra and recently disturbed sites by fire that had relatively low r^2, high RMSE and large bias.

Table 3. Evaluation of BESS, MODS, SVR and FLUXCOM in Alaska using r^2, RMSE, relative RMSE (rRMSE), bias and relative bias (rBias) across different PFTs. The units of RMSE and

bias are gC m^{-2} d^{-1}.

PFT	Sites	BESS GPP			MODIS GPP			SVR GPP			FLUXCOM GPP		
		r^2	RMSE (rRMSE)	Bias (rBias)	r^2	RMSE (rRMSE)	Bias (rBias)	r^2	RMSE (rRMSE)	Bias (rBias)	r^2	RMSE (rRMSE)	Bias (rBias)
ENF	6	0.82	1.01 (55%)	0.08 (4%)	0.81	1.06 (57%)	-0.06 (-3.2%)	0.75	1.29 (70%)	-0.55 (-30%)	0.88	0.77 (41%)	-0.01 (-5%)
DBF	1	0.93	0.68 (41%)	0.35 (21%)	0.95	0.57 (38%)	0.08 (5%)	0.54	1.9 (125%)	-0.85 (-56%)	0.96	0.86 (54%)	-0.42 (-28%)
Tundra	7	0.69	1.25 (184%)	0.67 (99%)	0.66	0.90 (151%)	0.24 (40%)	0.66	0.50 (85%)	-0.07 (-11%)	0.65	0.50 (85%)	-0.05 (-8%)
Fire	3	0.65	1.04 (95%)	0.51 (46%)	0.65	1.10 (106%)	0.39 (38%)	0.31	1.01 (98%)	-0.24 (23%)	0.68	0.66 (63%)	0.09 (8.7%)
Overall	17	0.74	1.12 (90%)	0.41 (33%)	0.75	1.01 (81%)	0.17 (14%)	0.65	1.07 (86%)	-0.27 (-22%)	0.85	0.69 (54%)	-0.07 (-6%)

In general, rRMSE was smaller in ENF and DBF compared to tundra and fire sites for all models, showing that model performance is still relatively weaker in tundra and fire sites. BESS and MODIS overestimated in tundra regions and underestimated in the boreal forest, whereas, SVR and FLUXCOM tended to underestimate GPP in tundra regions compared to boreal forest. In ENF, models

captured 75% to 88% of the variability in GPP, where rRMSE ranged from 41% to 70%. SVR, FLUXCOM and MODIS had negative rBiases in ENF, -30%, -5% and -3.2%, respectively, while BESS had a positive rBias of 4%. For DBF, models performed best in capturing over 90% of the variability in GPP, except for SVR, which also had the largest rRMSE (125%). Both BESS and MODIS showed a positive rBias (21% and 5%, respectively) while SVR and FLUXCOM exhibited a negative rBias (-56% and -28%, respectively) in DBF. In Tundra and Fire, the low productive sites, GPP was overestimated by the process-based and semi-empirical model, in contrast to the highly productive sites, ENF and DBF, whereas the machine-learning models underestimated GPP in all sites except fire, as illustrated in **Figure 2**. The data driven statistical models, clearly underestimated GPP with high relative biases in both ENF and DBF (SVR rBias = -56%, rRMSE = 70%; FLUXCOM rBias = -28%, rRMSE = 41%) but had a smaller relative bias in tundra and fire sites (SVR rBias = -11%, rRMSE = 85%; FLUXCOM rBias = -8%, rRMSE = 85%).

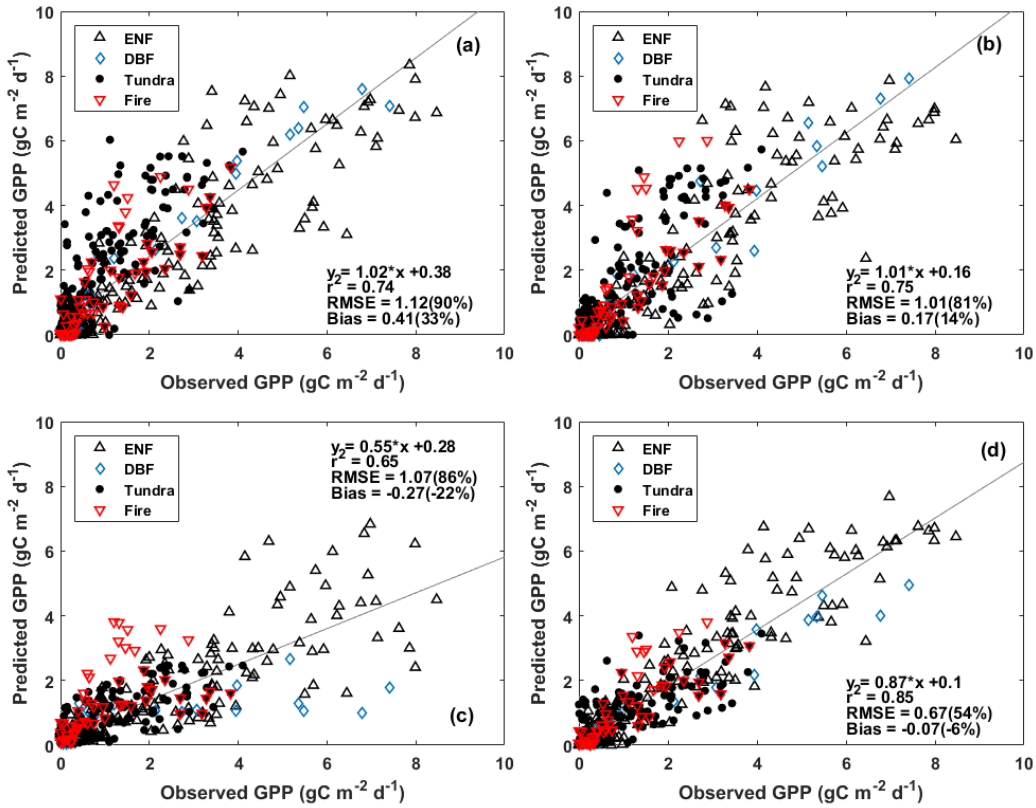

Figure 2 Evaluation of modeled GPP at a monthly time scale. (a) BESS, (b) MODIS, (c) SVR and (d) FLUXCOM with eddy covariance flux data. GPP from ENF and DBF sites are nearly twice of tundra GPP. GPP in fire and tundra sites are relatively much lower

3.2 IAV of GPP

We found that the boreal forest in Alaska had the largest magnitude of GPP IAV. DBF showed the largest magnitude of growing season GPP IAVs with the largest relative standard deviation of 13.9 ± 0.03%. The magnitude of GPP IAV in ENF is 13.4 ± 0.3% with the interior of Alaska exhibiting a greater variation compared to

the lower coastal regions of ENF. Fire showed a similar variability as ENF with a relative standard deviation of 12.8 ± 0.02%. Tundra had the lowest relative standard deviation of 10.6 ± 0.02%, with the Seward Peninsula and the north western part of North Slope exhibiting a higher magnitude in the variability of GPP. In contrast, the southern tundra regions and the other part of the northernmost region of Alaska showed the lowest degree of variability in GPP IAV (**Figure 3**). DBF is a highly productive area that has the most variation in the magnitude of GPP in the growing season. Furthermore, MODIS showed the highest degree of variation in all PFTs, followed by FLUXCOM, BESS and SVR which is a consequence of different approaches for each model leading to such variations (**Figure 4**). The boreal forest had the largest magnitude in the IAV of GPP with part of tundra regions also showing a high degree of variation, suggesting that vegetation production in these regions may contribute substantially to GPP IAV in Alaska.

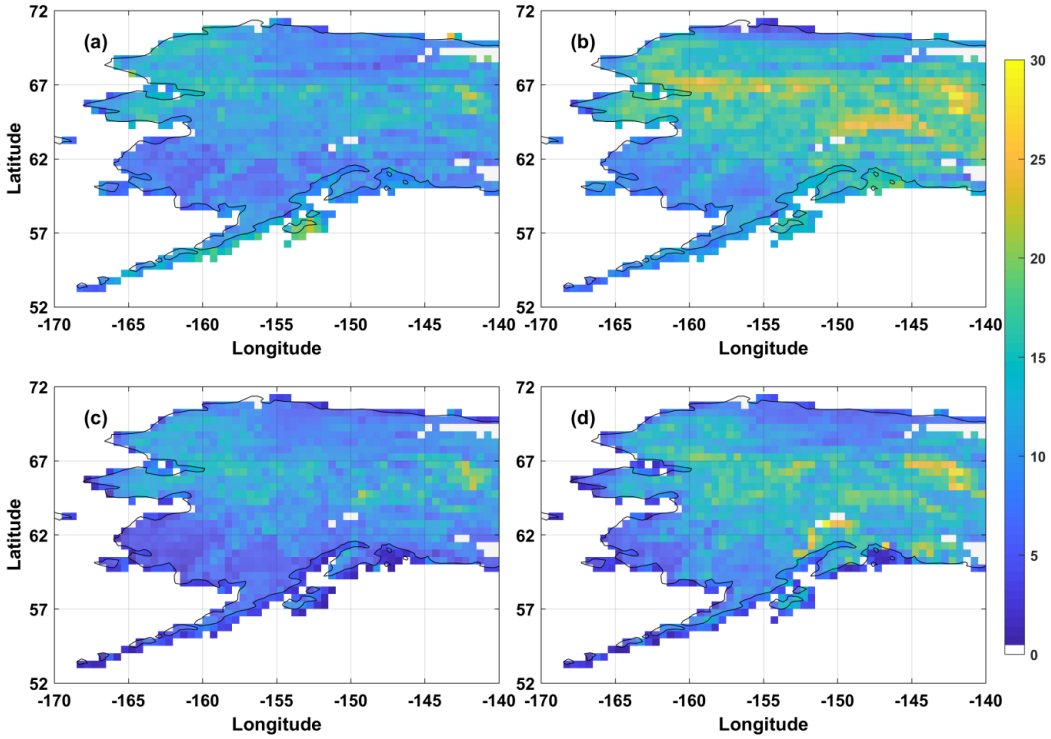

Figure 3 The Relative standard deviation (%) of GPP IAV (a) BESS, (b) MODIS, (c) SVR and (d) FLUXCOM.

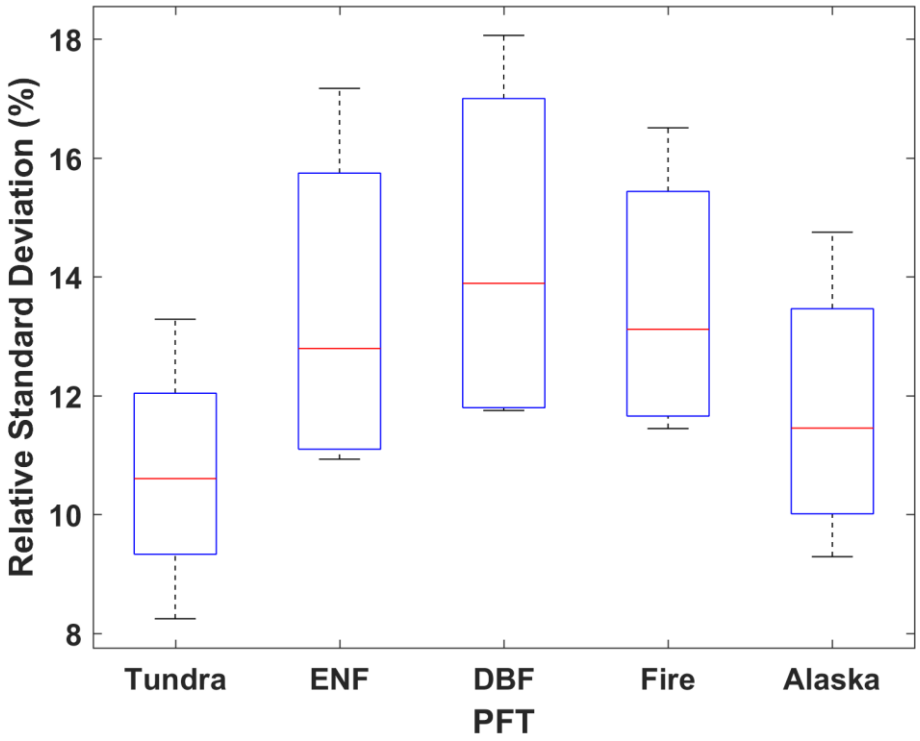

Figure 4 Averaged relative standard deviation of GPP IAV.

The pattern of growing season GPP IAV was similar across the different PFTs with varying magnitudes (**Figure 6**), except for fire areas in SVR. Tundra had the highest relative contribution to the interannual variation of GPP with the largest fraction of 55%, exceeding ENF (38%), DBF (7%) and fire (0.8%) in Alaska (**Figure 6a**). All of the models, BESS, MODIS, SVR and FLUXCOM, displayed a similar spatial and temporal pattern in the IAV of growing season GPP. The spatial pattern of the relative contribution of each pixel to growing season GPP IAV varied

across the region of Alaska. The growing season GPP mean is relatively small in tundra compared to the other PFTs, but tundra in the Seward Peninsula and western part of the North Slope contributed up to 0.2% of the IAV of GPP growing season, which is similar to the relative contribution of pixels in DBF to GPP IAV. Overall, the sum of relative pixel contribution for each PFTs show that tundra contributed the most to the IAV of GPP as it covered up to 68% of Alaska (**Figure 6b**). Despite the magnitude of the flux in PFTs, the percent of land cover fraction for each respective PFT cover resulted in contributing most to the IAV of GPP. 0.06 %, 0.03%, 0.05% and 0.03% of the pixels had negative relative contribution to GPP IAV for BESS, MODIS, SVR and FLUXCOM, respectively. The negative relative contributions were generally located in the north eastern alpine regions of Alaskan. BESS and SVR showed more negative relative contribution in the southern tail of Alaska.

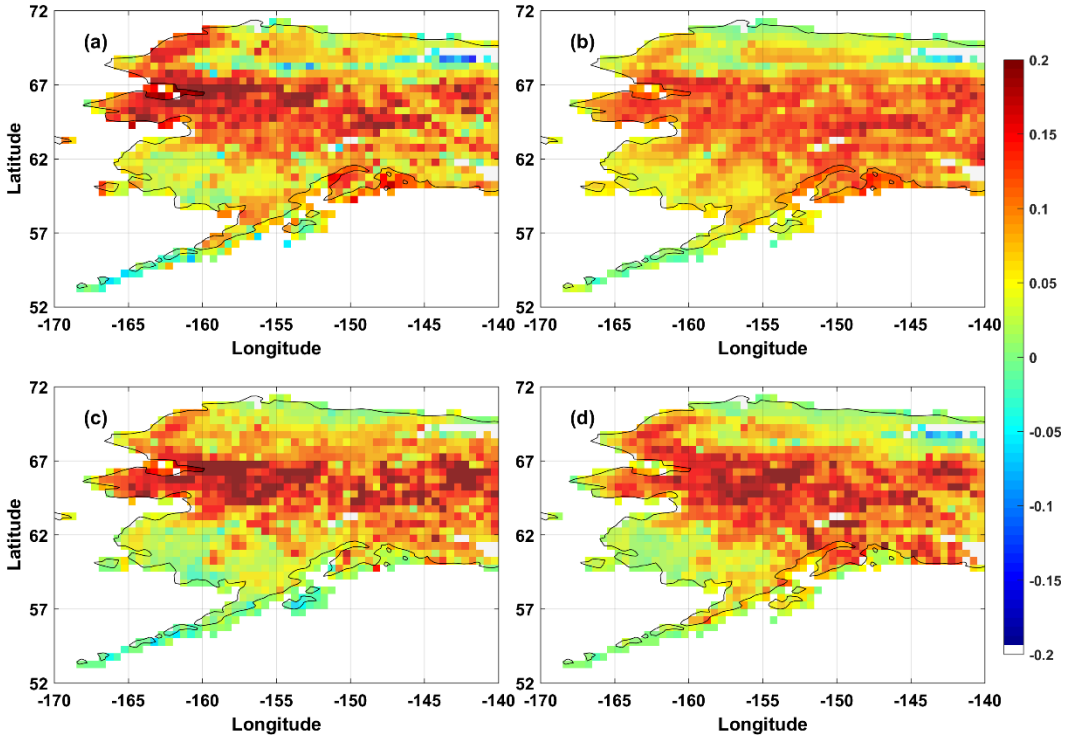

Figure 5 Relative contribution (%) of each grid cell to GPP IAV. (a) BESS, (b) MODIS. (c) SVR and (d) FLUXCOM.

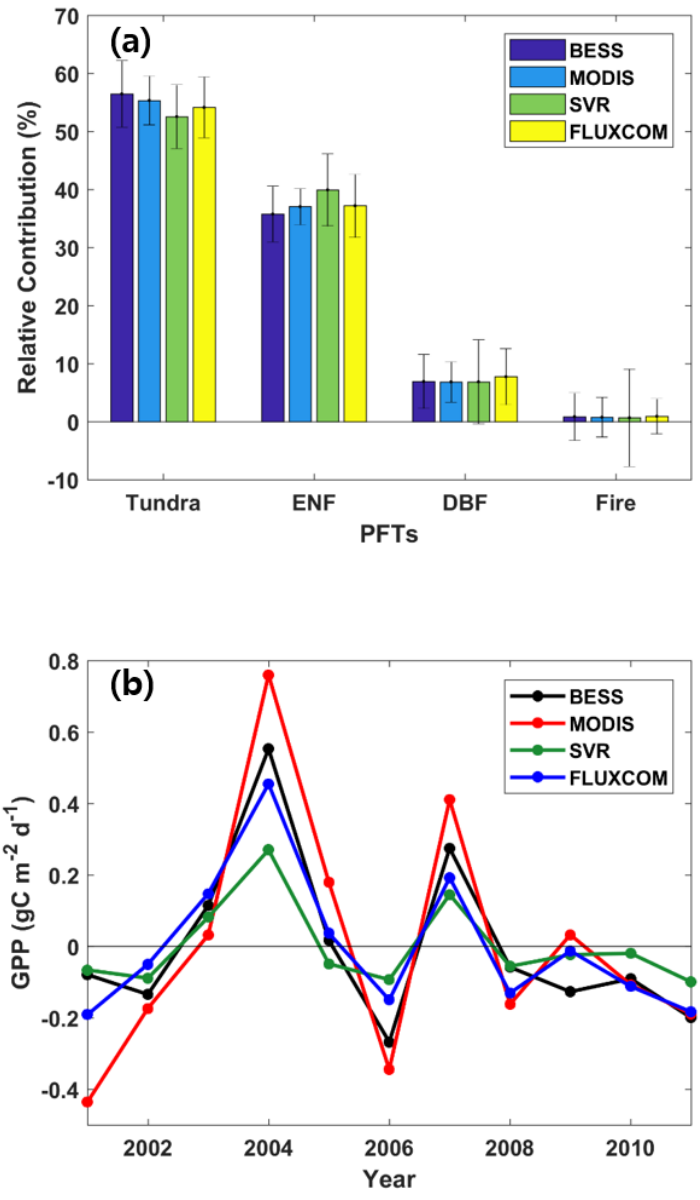

Figure 6 (a) The sum of relative contribution of GPP IAV each PFT, and the (b) the IAV of GPP from 2001 to 2011 in Alaska.

The year to year relative contribution of PFT to GPP IAV varies where Tundra was the major contributor followed by ENF, DBF and Fire (**Figure 7**). All models show that Tundra was the major contributor to GPP IAV in 2001, 2002, 2004, 2005, 2006, 2008, 2009, 2010, 2011, 2012, whereas ENF contributed most to GPP IAV in 2003 and 2008 when GPP anomaly was close to the mean. DBF and Fire contributed to the IAV of GPP every year in relatively smaller quantity due to its smaller area. In the warmer years the relative contribution of PFT to GPP IAV was positive while in the colder years the relative contribution of PFT to GPP IAV was negative.

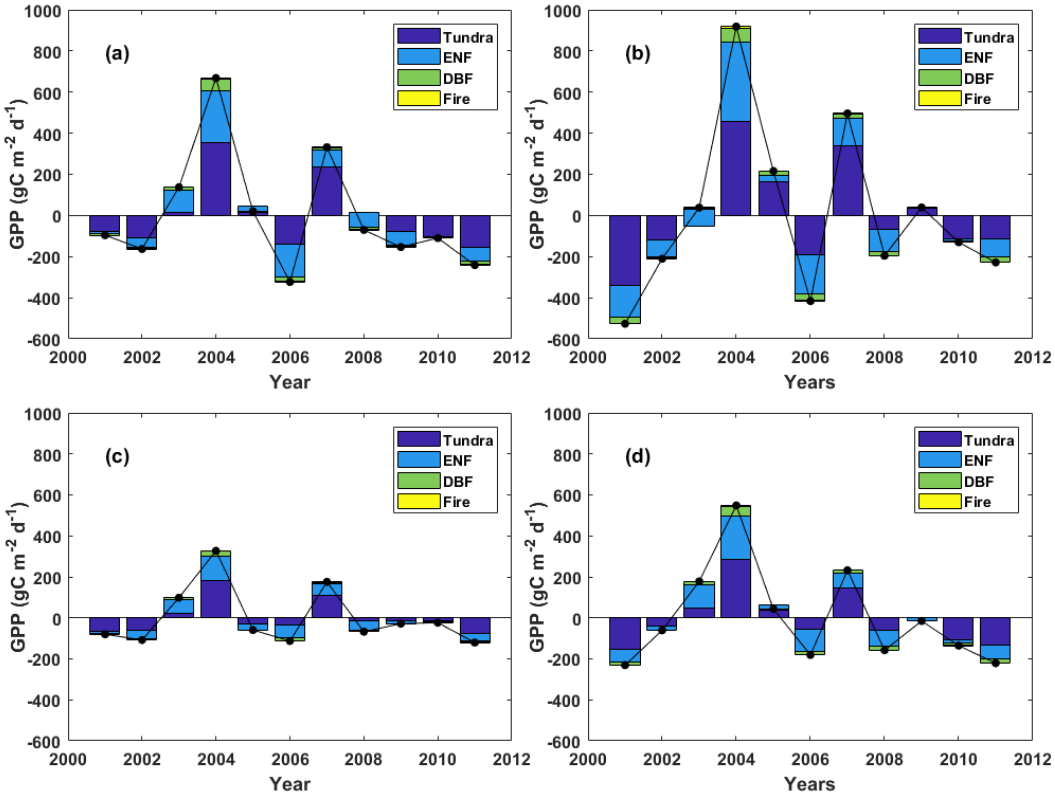

Figure 7 Relative contribution of PFT to GPP. (a) BESS, (b) MODIS. (c) SVR and (d) FLUXCOM. The black line indicates GPP anomaly for each year over Alaska

3.3 Relationship between IAV of GPP and Climate Variables

Air temperature was the most dominant driver of the spatial and temporal pattern of GPP IAV for all PFTs. As illustrated in **Figure 8,** the spatial pattern between air temperature and GPP was similar, where 81%, 87%, 78%, 82% of the

pixels had a significant (*p Value* < 0.1) partial correlation for BESS, MODIS, SVR and FLUXCOM, respectively, of which more than 50% of the pixels were located in tundra, 20 % in ENF, 0.04 % in DBF and 0.005 % in the fire regions. Across all PFTs, air temperature had the highest positive correlation followed by radiation, indicating that the high latitude ecosystems are co-limited by both air temperature and shortwave radiation (**Figure 8**). In Alaska, it is interesting to note that GPP in the northern tip of Alaska is not driven by air temperature but solar radiation (**Figure 8**). In contrast, there are much fewer areas that are affected by precipitation, with only about 16 – 18% of the pixels showing a significant (*p Value* < 0.1) partial correlation coefficient. There is a decrease of GPP when there is precipitation in the northern most part of tundra and the southern part of coastal tundra, which emphasize that tundra GPP does not depend on snowfall and rain for water as these regions are underlain by permafrost.

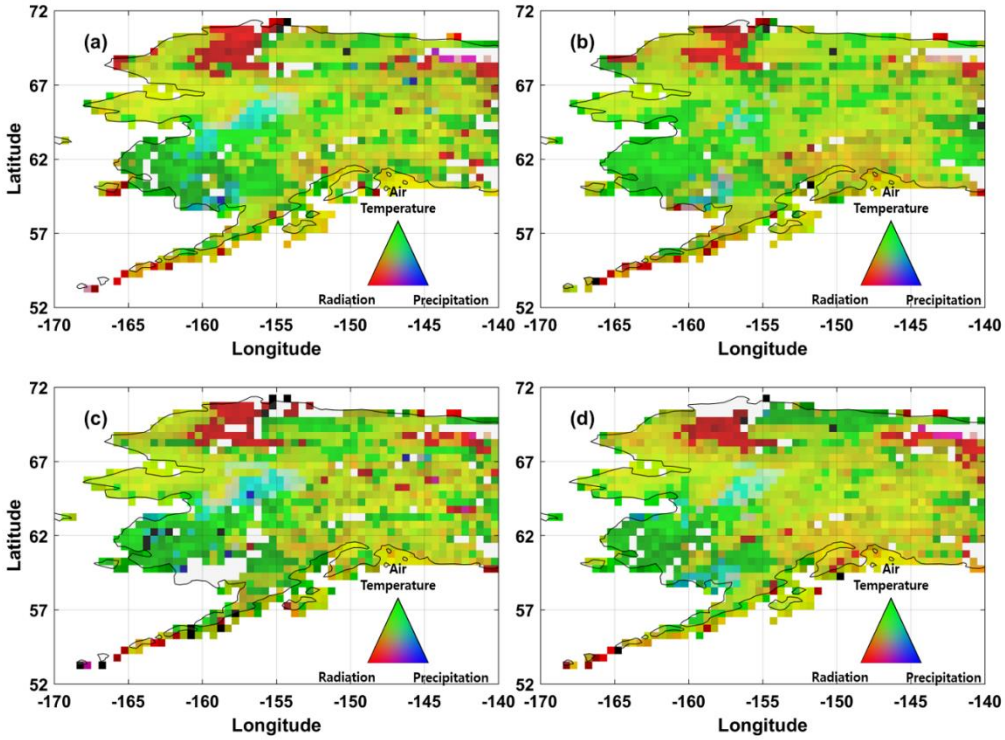

Figure 8 RGB composite of climatic drivers

As illustrated in **Figure 5**, the Seward Peninsula and the western North Slope contributed up to 0.2% of GPP IAV, which is similar to the pixels in the boreal forest that is found in the Interior of Alaska. In contrast, the contribution of the Arctic Coastal Plain and North Slope of Alaska and southern tundra in Alaska to GPP was smaller than 0.1%. The spatial pattern of relative contribution to GPP IAV is remarkably similar to the areas where both air temperature and radiation drive GPP (**Figure 8**). The Arctic Coastal Plain and southern tundra regions, which has a

partial correlation coefficient with air temperature contributed less to GPP IAV than the areas where both air temperature and radiation have a relationship with GPP. West of the Brooks Range, the alpine regions, and Alaska Peninsula show a small negative contribution to air temperature corresponding to the positive correlations with precipitation. The relative contribution of pixels to GPP in BESS, MODIS, SVR and FLUXCOM was associated with both air temperature and radiation, displaying a similar pattern although they had different spatial pattern and magnitude (**Figure 9**). The negative relative contribution is from tundra when the driving factors are both radiation and precipitation. Air temperature and radiation were co-dominantly associated to the GPP IAV for all PFTs in Alaska. At one point in the growing season, daylight hours may be up to 24 hours, which may enhance vegetation productivity (Bliss *et al.,* 1973). Across the PFTs for Alaska air temperature and radiation were the most important climate factors that influence GPP year to year variability.

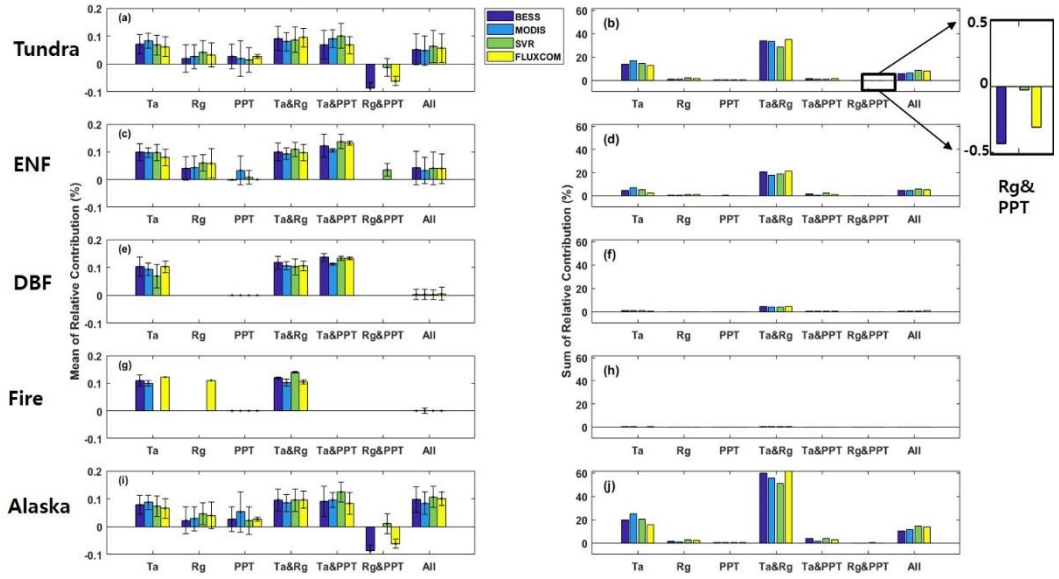

Figure 9 The mean and sum of relative contribution to GPP IAV for PFT. Mean of relative contribution for a) Tundra c) ENF e) DBF g) Fire and i) Alaska and the sum of relative contribution in b) Tundra d) ENF f) DBF h) Fire and j) Alaska when there is a partial correlation with Ta (air temperature), Rg (radiation), PPT (precipitation), Ta & Rg (air temperature and radiation), Ta & PPT (air temperature and precipitation), Rg & PPT (radiation and precipitation) and All (air temperature, precipitation and radiation). The error bar shows the variation of relative contribution for each case.

The average partial correlation coefficient for the whole of Alaska shows that growing season GPP was positively correlated to growing season temperature (r = 0.8) and radiation (r = 0.7) but a small negative correlation with precipitation (r = -0.2). Except for MODIS, the other models show that only DBF has a positive correlation coefficient with precipitation. In the fire region, BESS, SVR and FLUXCOM GPP were not associated with precipitation, implying that these

ecosystems recover from fire disturbance regardless of precipitation. There is high variation in precipitation correlation coefficient with GPP. The relationships between growing season GPP and climate variables vary greatly among PFTs but these results highlight that both air temperature and shortwave radiation are the limiting factor that act together upon GPP to control its year to year variation.

4. Discussion

4.1 Model Performance across different PFTs

The performance of BESS, MODIS, SVR and FLUXCOM at a site scale across PFTs differed substantially, where all models showed a better performance in the boreal forest compared to tundra and fire sites (**Table 3**). BESS, MODIS, SVR and FLUXCOM could capture 65% to 85% of the seasonal variability in GPP but they had a larger uncertainty in tundra compared to boreal forest. Fisher *et al.,* (2014) reported that GPP had the second highest uncertainty (225%) among the different carbon flux components after soil carbon from terrestrial biosphere models, where tundra exhibited more uncertainty compared to boreal forest (Ueyama *et al.,* 2013, Tramontana *et al.,* 2016). One precaution to take in model evaluation is that the eddy covariance flux towers could not represent all the ecosystems in Alaska, which has a highly heterogeneous landscape and topography (Williams *et al.,* 2006, Shaver *et al.,* 2007). Our model evaluation did not include eddy covariance flux towers situated in white spruce and birch forests, various aged ecosystems after fire, wetlands, bogs and other types of shrubland (Flemming 1997, Walker *et al.,* 2005). There was one DBF site (white spruce forest) and tundra sites were only located in the northern region of Alaska (**Figure 1**), thus excluding tundra ecosystems composed of tall or low shrubs, alpine or moist herbaceous tundra.

Model evaluation revealed that the data driven models tended to underestimate

GPP, whereas the process-based and semi-empirical models tended to overestimate GPP in Alaska. SVR and FLUXCOM are limited by data, which were from only a few types of arctic ecosystems with most of the data available in the growing season (Kwon *et al.*, 2006, Ueyama *et al.*, 2013). FLUXCOM used 224 flux tower sites from FLUXNET La Thulie synthesis dataset of which 6 sites were located in Alaska. There are 3 sites found in the Alaskan Arctic tundra regions (Atqasuk, Barrow and Ivotuk) and the other 3 in the Alaska boreal forest regions (Bonzona Creek 1, Bonzona Creek 2 and Bonzona Creek 3). In contrast, SVR upscaled from 21 flux tower sites to a regional scale in Alaska, but showed the least spatial and temporal variation of GPP. Moreover, GPP data is an indirect measurement of the eddy covariance system, thus it is subject to uncertainties in the flux partitioning methods. Turner *et al.,* (2006) traced the overestimation of MODIS GPP in tundra biomes to unrealistically high values of fPAR (fraction of absorbed photosynthetically active radiation) and underestimation of GPP in highly productive sites (i.e. DBF and ENF) due to low values of vegetation LUE (Light Use Efficiency). There have been significant improvements and updates of MODIS fPAR, including the removal of cloud contamination, but studies still show that estimation of GPP with MODIS fPAR and maximum LUE from the biome look-up-table has uncertainty in capturing seasonal and yearly variation (Sjöström *et al.,* 2013, Cheng *et al.,* 2014, Wang *et al.,* 2017). Cheng *et al.,* (2014) demonstrated that GPP estimated using

fPAR, from chlorophyll in leaves, and site-specific maximum LUE resulted in a higher accuracy than GPP derived from MODIS fPAR and maximum LUE from the biome look-up-table. Recently, an evaluation of the latest MOD17A2H GPP that is derived from the most updated MODIS products, still traced the sources of error to MODIS fPAR (MOD15A2H Collection 6), LUE and landcover misclassification (Wang et al., 2017). Not only BESS and MODIS used MODIS fPAR products but also SVR and FLUXCOM, which may have led to such high uncertainty in tundra. The key photosynthesis parameter in BESS is V_{cmax} (maximum carboxylation rate) and LAI, which may have also led to bias and error in the estimation of GPP. The high error and bias in BESS may be due to the largely unavailable V_{cmax} data in the Arctic (Rogers 2014), where other terrestrial biosphere models are also still found to underestimate the photosynthetic capacity and CO_2 assimilation due to this parameter (Walker *et al.,* 2014, Rogers *et al.,* 2017). Hence tundra still remains a challenging PFT for both process-based and machine-learning approaches.

4.2 IAV of GPP

The IAV of GPP had a similar pattern with the IAV of air temperature and radiation, where all models showed a consistent spatial and temporal pattern of GPP IAV from 2001 to 2011 (**Figure 3** and **Figure 10**). Other studies have also reported a similar IAV of GPP in Alaska (Ueyama *et al.,* 2013, Mekonnen *et al.,* 2016).

Mekonnen *et al.,* (2016) reported the GPP IAV in North America was related with the cold phase of El Niño Southern Oscillation (ENSO) and negative Multivariate ENSO Index that has led to major droughts in 2001, 2002, 2008 and 2009, leading to small GPP anomalies. The results also show that that there were small or negative GPP anomalies during 2001, 2002, 2008 and 2009 (**Figure 11**). In contrast, during the warmer years GPP anomalies were positive, especially during 2004 and 2007 which were recorded as particularly warm and dry years with many fire events.

Overall, the boreal forest exhibited a larger variability of GPP than in tundra, which may be explained by the complexity of the canopy structure (**Figure 3**) (Zhou *et al.,* 2017). The complexity of canopy structure increases with a non-linear change in biomass, cover and height of the understory and overstory, as we transition from tundra to shrub tundra to closed canopy forest (Thompson et al., 2004, Beringer et al., 2005). In particular, the understory variation increases significantly along the gradient from tundra to forest. A previous study shows that in a sparsely populated ENF, the seasonal variation of the understory vegetation contributed significantly to the IAV of GPP as it was more responsive to the environmental controlling factors (Ueyama *et al.,* 2006). Therefore, the higher variability of GPP in the boreal forest could be explained by the larger biomass of the forest and the high variability of the understory canopy. Furthermore, the various stand age of the forest contributes to

the larger variation of GPP in the boreal forest (Goulden *et al.,* 2006). Our results show that tundra contributed most to the IAV of GPP with up to 55%, which is expected as it was the largest PFT covering 68% of Alaska. The relative contribution of tundra to GPP IAV is relatively less because of the negative contribution of tundra in the north eastern Brooks Range and Alaska Peninsular to GPP IAV (**Figure 3**). In contrast, ENF contribution (38%) is relatively higher to GPP IAV than its area (26%) as their average relative contribution was higher than tundra with no negative contribution.

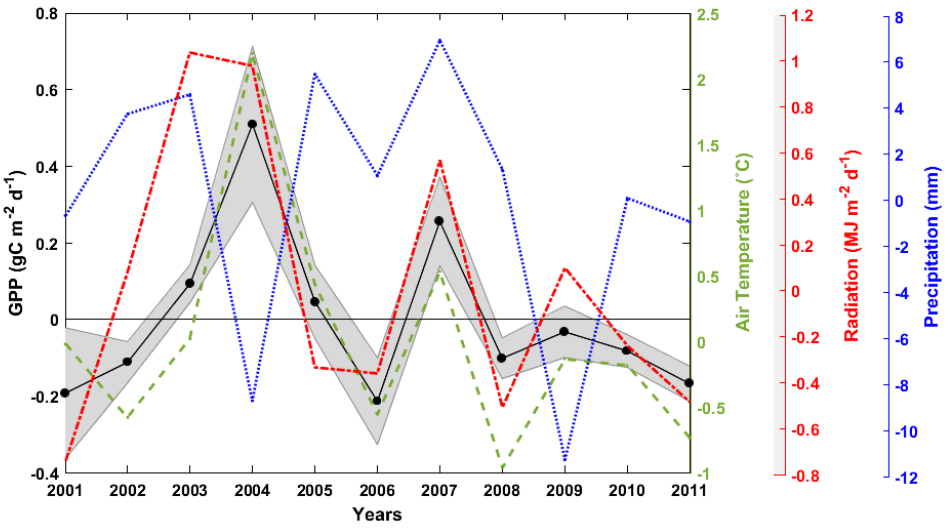

Figure 10 The IAV pattern of GPP (black solid line) in Alaska from 2001 to 2011 with air temperature (green dashed line), precipitation (red dotted line) and radiation (blue dotted and dashed line). The black solid line represents the ensemble of BESS, MODIS, SVR and FLUXCOM while the shaded area in grey represents the variation of the models.

4.3 Controlling factors in IAV of GPP

We found that GPP IAV in Alaska was driven by both air temperature and radiation across all PFTs (**Figure 8** and **Figure11**). This is in agreement with other research showing that the northern vegetation is most sensitive to air temperature and radiation (Nemani et al., 2003, Mekonnen et al., 2016, Seddon et al., 2016, Liang et al., 2017). Light use efficiency increases with temperature, only in cold regions. This may explain why GPP IAV was co-limited by air temperature and radiation across PFTs where the efficiency of vegetation transforming absorbed radiation into plant biomass is enhanced with increasing temperature (Schwalm et al., 2006, Garbulsky et al., 2010). Ueyama et al., (2006) also reported that light use efficiency was limited by low temperatures in a black spruce forest. In Alaska, when air temperature increases vegetation productivity could be enhanced by efficiently absorbing radiation compared to colder years.

5. Conclusion

In this study we examined the spatial and temporal IAV of GPP across Alaska from 2001 to 2011 using four satellite based GPP products. Model performance differed substantially among PFTs, showing a better performance in the boreal forest compared to tundra. GPP in tundra had the largest relative contributed to the IAV of GPP as it has the largest area among PFTs. In particular, GPP from tundra in the Seward Peninsula and the western Brooks Range highly contributed to IAV of GPP along with the interior of Alaska. The spatial and temporal variation of GPP IAV was relatively higher in the boreal forest than tundra. The relationships between GPP and climate variables vary among PFTs depending on the region due to topography, but both air temperature and radiation were the major climate variables that governed GPP to control its year to year variation. This study highlights that vegetation response is sensitive to air temperature and radiation IAV, which controls the year to year spatial and temporal variability of GPP. Therefore, in the high latitudes, warming or cooling as a result of climate change could significantly impact the magnitude and trajectory of the IAV of land-atmosphere interaction of carbon dioxide.

References

Ahlström, A., M. R. Raupach, Guy Schurgers, Benjamin Smith, Almut Arneth, Martin Jung, Markus Reichstein, JosepG. Canadell, Pierre Friedlingstein, Atul K. Jain, Etsushi Kato, Benjamin Poulter, Stephen Sitch, Benjamin D. Stocker, Nicolas Viovy, Ying Ping Wang, Andy Wiltshire, Sönke Zaehle and N. Zeng1 (2015). "The dominant role of semi-arid ecosystems in the trend and variability of land CO_2 sink." Science **348**(637): 895-899.

Beck, P. S. A. and S. J. Goetz (2012). "Corrigendum: Satellite observations of high northern latitude vegetation productivity changes between 1982 and 2008: ecological variability and regional differences." Environmental Research Letters **7**(2): 029501. DOI: 10.1088/1748-9326/7/2/029501

Bekryaev, R. V., I. V. Polyakov and V. A. Alexeev (2010). "Role of Polar Amplification in Long-Term Surface Air Temperature Variations and Modern Arctic Warming." Journal of Climate **23**(14): 3888-3906. DOI: 10.1175/2010jcli3297.1

Beringer, J., F. S. Chapin, C. C. Thompson and A. D. McGuire (2005). "Surface energy exchanges along a tundra-forest transition and feedbacks to climate." Agricultural and Forest Meteorology **131**(3-4): 143-161. DOI: 10.1016/j.agrformet.2005.05.006

Bieniek, P. A. and J. E. Walsh (2017). "Atmospheric circulation patterns associated with monthly and daily temperature and precipitation extremes in Alaska." International Journal of Climatology. DOI: 10.1002/joc.4994

Black, T. A., W. J. Chen, A. G. Barr, M. A. Arain, Z. Chen, Z. Nesic, E. H. Hogg, H. H. Neumann and P. C. Yang (2000). "Increased carbon sequestration by a boreal deciduous forest in years with a warm spring." Geophysical Research Letters **27**(9): 1271-1274. DOI: 10.1029/1999gl011234

Bliss, L. C., G. M. Courtin, D. L. Pattie, R. R. Riewe, D. W. A. Whitfield and P. Widden (1973). "Arctic and tundra ecosystems." Annu. Rev. Ecol. Syst **4**: 359-399.

ChapinIII, F. S., M. Sturm, M. C. Serreze, J. P. McFadden, J. R. Key, A. H. Lloyd, A. D. McGuire, T. S. Rupp, A. H. Lynch, J. P. Schimel, J. Beringer, W. L. Chapman, H. E. Epstein, E. S. Euskirchen, L. D. Hinzman, G. Jia, C.-L. Ping, K. D. Tape, C. D. C. Thompson, D. A. Walker and J. M. Welker (2005). "Role of Land-Surface Changes in Arctic Summer Warming." Science **310**(5748): 657 - 660.

Cheng, Y.-B., Q. Zhang, A. I. Lyapustin, Y. Wang and E. M. Middleton (2014). "Impacts of light use efficiency and fPAR parameterization on gross primary production modeling." Agricultural and Forest Meteorology **189-190**: 187-197. DOI: 10.1016/j.agrformet.2014.01.006

Commane, R., J. Lindaas, J. Benmergui, K. A. Luus, R. Y. Chang, B. C. Daube, E. S. Euskirchen, J. M. Henderson, A. Karion, J. B. Miller, S. M. Miller, N. C. Parazoo, J. T. Randerson, C. Sweeney, P.

Tans, K. Thoning, S. Veraverbeke, C. E. Miller and S. C. Wofsy (2017). "Carbon dioxide sources from Alaska driven by increasing early winter respiration from Arctic tundra." Proc Natl Acad Sci U S A. DOI: 10.1073/pnas.1618567114

Cramer, W., D.W.Kicklighter, A.Bondeau, B. M. III, G. Churkina, B.Nemry, A.Ruimy and A.L.Schloss (1999). "Comparing Global Models of Terrestrial Net Primary Productivity: overview and key results." Glob Chang Biol **5**: 1 - 15.

Euskirchen, E. S., M. S. Bret-Harte, G. J. Scott, C. Edgar and G. R. Shaver (2012). "Seasonal patterns of carbon dioxide and water fluxes in three representative tundra ecosystems in northern Alaska." Ecosphere **3**(1): art4. DOI: 10.1890/es11-00202.1

Euskirchen, E. S., M. S. Bret-Harte, G. R. Shaver, C. W. Edgar and V. E. Romanovsky (2016). "Long-Term Release of Carbon Dioxide from Arctic Tundra Ecosystems in Alaska." Ecosystems. DOI: 10.1007/s10021-016-0085-9

Farquhar, G. D., S. v. Caemmerer and J. A. Berry (1980). "A biochemical model of photosynthetic CO_2 assimilation in leaves of C_3 species." Planta **149**: 78 - 90.

Fisher, J. B., M. Sikka, W. C. Oechel, D. N. Huntzinger, J. R. Melton, C. D. Koven, A. Ahlström, M. A. Arain, I. Baker, J. M. Chen, P. Ciais, C. Davidson, M. Dietze, B. El-Masri, D. Hayes, C. Huntingford, A. K. Jain, P. E. Levy, M. R. Lomas, B. Poulter, D. Price, A. K. Sahoo, K. Schaefer, H. Tian, E. Tomelleri, H. Verbeeck, N. Viovy, R. Wania, N. Zeng and C. E. Miller (2014). "Carbon cycle uncertainty in the Alaskan Arctic." Biogeosciences **11**(15): 4271-4288. DOI: 10.5194/bg-11-4271-2014

Flemming, M. (1997). "A statewide vegetation map of Alaska using phenological classificaiton of AVHRR data. In: Proceedings of the Second Circumpolar Arctic Vegetation Mapping Workshop, Arendal, Norway." 25-26.

Garbulsky, M. F., J. Peñuelas, D. Papale, J. Ardö, M. L. Goulden, G. Kiely, A. D. Richardson, E. Rotenberg, E. M. Veenendaal and I. Filella (2010). "Patterns and controls of the variability of radiation use efficiency and primary productivity across terrestrial ecosystems." Global Ecology and Biogeography **19**(2): 253-267. DOI: 10.1111/j.1466-8238.2009.00504.x

Goulden, M. L., G. C. Winston, A. M. S. McMillan, M. E. Litvak, E. L. Read, A. V. Rocha and J. Rob Elliot (2006). "An eddy covariance mesonet to measure the effect of forest age on land-atmosphere exchange." Global Change Biology **12**(11): 2146-2162. DOI: 10.1111/j.1365-2486.2006.01251.x

Goulden, M. L., S. Wofsy, J. W. Harden, S. E. Trumbore, P. M. Crill, S. T. Gower, T. Fries, B. C. Daube, S. M. Fan, D. J. Sutton, A. Bazzaz and J. W. Munger (1998). "Sensitivity of Boreal Forest C

balance to soil thaw." Science **279**: 214-217.

Guay, K. C., P. S. Beck, L. T. Berner, S. J. Goetz, A. Baccini and W. Buermann (2014). "Vegetation productivity patterns at high northern latitudes: a multi-sensor satellite data assessment." Glob Chang Biol **20**(10): 3147-3158. DOI: 10.1111/gcb.12647

Harazono, Y., M. Mano, A. Miyata and R. C. Zulueta (2003). "Interannual carbon dioxide uptake of a wet sedge tundra ecosystem in the Arctic." Tellus **55B**: 215-231.

Harris, I., P. D. Jones, T. J. Osborn and D. H. Lister (2014). "Updated high-resolution grids of monthly climatic observations - the CRU TS3.10 Dataset." International Journal of Climatology **34**(3): 623-642. DOI: 10.1002/joc.3711

Huntzinger, D. N., C. Schwalm, A. M. Michalak, K. Schaefer, A. W. King, Y. Wei, A. Jacobson, S. Liu, R. B. Cook, W. M. Post, G. Berthier, D. Hayes, M. Huang, A. Ito, H. Lei, C. Lu, J. Mao, C. H. Peng, S. Peng, B. Poulter, D. Riccuito, X. Shi, H. Tian, W. Wang, N. Zeng, F. Zhao and Q. Zhu (2013). "The North American Carbon Program Multi-Scale Synthesis and Terrestrial Model Intercomparison Project – Part 1: Overview and experimental design." Geoscientific Model Development **6**(6): 2121-2133. DOI: 10.5194/gmd-6-2121-2013

Ito, A., M. Inatomi, D. N. Huntzinger, C. Schwalm, A. M. Michalak, R. Cook, A. W. King, J. Mao, Y. Wei, W. M. Post, W. Wang, M. A. Arain, S. Huang, D. J. Hayes, D. M. Ricciuto, X. Shi, M. Huang, H. Lei, H. Tian, C. Lu, J. Yang, B. Tao, A. Jain, B. Poulter, S. Peng, P. Ciais, J. B. Fisher, N. Parazoo, K. Schaefer, C. Peng, N. Zeng and F. Zhao (2016). "Decadal trends in the seasonal-cycle amplitude of terrestrial CO2 exchange resulting from the ensemble of terrestrial biosphere models." Tellus B: Chemical and Physical Meteorology **68**(1): 28968. DOI: 10.3402/tellusb.v68.28968

Iwata, H., Y. Harazono and M. Ueyama (2012). "The role of permafrost in water exchange of a black spruce forest in Interior Alaska." Agricultural and Forest Meteorology **161**: 107-115. DOI: 10.1016/j.agrformet.2012.03.017

Iwata, H., M. Ueyama, Y. Harazono, S. Tsuyuzaki, M. Kondo and M. Uchida (2011). "Quick Recovery of Carbon Dioxide Exchanges in a Burned Black Spruce Forest in Interior Alaska." Sola **7**: 105-108. DOI: 10.2151/sola.2011-027

Jeong, S.-J., C.-H. Ho, H.-J. Gim and M. E. Brown (2011). "Phenology shifts at start vs. end of growing season in temperate vegetation over the Northern Hemisphere for the period 1982-2008." Global Change Biology **17**(7): 2385-2399. DOI: 10.1111/j.1365-2486.2011.02397.x

Jiang, C. and Y. Ryu (2016). "Multi-scale evaluation of global gross primary productivity and evapotranspiration products derived from Breathing Earth System Simulator (BESS)." Remote Sensing of Environment **186**: 528-547. DOI: 10.1016/j.rse.2016.08.030

Kwon, H.-J., W. C. Oechel, R. C. Zulueta and S. J. Hastings (2006). "Effects of climate variability on carbon sequestration among adjacent wet sedge tundra and moist tussock tundra ecosystems." Journal of Geophysical Research **111**(G3). DOI: 10.1029/2005jg000036

Liang, W., Y. Lu, W. Zhang, S. Li, Z. Jin, P. Ciais, B. Fu, S. Wang, J. Yan, J. Li and H. Su (2017). "Grassland gross carbon dioxide uptake based on an improved model tree ensemble approach considering human interventions: global estimation and covariation with climate." Glob Chang Biol **23**(7): 2720-2742. DOI: 10.1111/gcb.13592

McGuire, A. D., F. S. Chapin, J. E. Walsh and C. Wirth (2006). "Integrated Regional Changes in Arctic Climate Feedbacks: Implications for the Global Climate System*." Annual Review of Environment and Resources **31**(1): 61-91. DOI: 10.1146/annurev.energy.31.020105.100253

Mekonnen, Z. A., R. F. Grant and C. Schwalm (2016). "Contrasting changes in gross primary productivity of different regions of North America as affected by warming in recent decades." Agricultural and Forest Meteorology **218-219**: 50-64. DOI: 10.1016/j.agrformet.2015.11.016

Molau, U. and P. Molgaard (1996). "International Tundra Experiment Mannual." Danish Polar Center, Copenhagen, Denmark.

Nakai, T., Y. Kim, R. C. Busey, R. Suzuki, S. Nagai, H. Kobayashi, H. Park, K. Sugiura and A. Ito (2013). "Characteristics of evapotranspiration from a permafrost black spruce forest in interior Alaska." Polar Science **7**(2): 136-148. DOI: 10.1016/j.polar.2013.03.003

Nauta, A. L., M. M. P. D. Heijmans, D. Blok, J. Limpens, B. Elberling, A. Gallagher, B. Li, R. E. Petrov, T. C. Maximov, J. van Huissteden and F. Berendse (2014). "Permafrost collapse after shrub removal shifts tundra ecosystem to a methane source." Nature Climate Change **5**(1): 67-70. DOI: 10.1038/nclimate2446

Nemani, R. R., C. D. Keeling, H. Hashimoto, W. M. Jolly, S. C. Piper, C. J. Tucker, R. B. Myneni and S. W. Running (2003). "Climate-driven increases in global terrestrial net primary production from 1982 to 1999." Science **300**(5625): 1560-1563. DOI: 10.1126/science.1082750

Oechel, W. C., S. J. Hastings, G. Vourlitis, M. Jenkins, G. Riecher and N. Grulke (1993). "Recent changes of the arctic tundra ecosystem from a net carbon dioxide sink to source." Nature Lett. **361**: 520 - 523.

Park, H., S.-J. Jeong, C.-H. Ho, J. Kim, M. E. Brown and M. E. Schaepman (2015). "Nonlinear response of vegetation green-up to local temperature variations in temperate and boreal forests in the Northern Hemisphere." Remote Sensing of Environment **165**: 100-108. DOI: 10.1016/j.rse.2015.04.030

Park, T., S. Ganguly, H. Tømmervik, E. S. Euskirchen, K.-A. Høgda, S. R. Karlsen, V. Brovkin, R. R. Nemani and R. B. Myneni (2016). "Changes in growing season duration and productivity of northern vegetation inferred from long-term remote sensing data." Environmental Research Letters **11**(8): 084001. DOI: 10.1088/1748-9326/11/8/084001

Piao, S., P. Ciais, P. Friedlingstein, P. Peylin, M. Reichstein, S. Luyssaert, H. Margolis, J. Fang, A. Barr, A. Chen, A. Grelle, D. Y. Hollinger, T. Laurila, A. Lindroth, A. D. Richardson and T. Vesala (2008). "Net carbon dioxide losses of northern ecosystems in response to autumn warming." Nature **451**(7174): 49-52. DOI: 10.1038/nature06444

Piao, S., Z. Liu, T. Wang, S. Peng, P. Ciais, M. Huang, A. Ahlstrom, J. F. Burkhart, F. Chevallier, I. A. Janssens, S.-J. Jeong, X. Lin, J. Mao, J. Miller, A. Mohammat, R. B. Myneni, J. Peñuelas, X. Shi, A. Stohl, Y. Yao, Z. Zhu and P. P. Tans (2017). "Weakening temperature control on the interannual variations of spring carbon uptake across northern lands." Nature Climate Change **7**(5): 359-363. DOI: 10.1038/nclimate3277

Piao, S., H. Nan, C. Huntingford, P. Ciais, P. Friedlingstein, S. Sitch, S. Peng, A. Ahlstrom, J. G. Canadell, N. Cong, S. Levis, P. E. Levy, L. Liu, M. R. Lomas, J. Mao, R. B. Myneni, P. Peylin, B. Poulter, X. Shi, G. Yin, N. Viovy, T. Wang, X. Wang, S. Zaehle, N. Zeng, Z. Zeng and A. Chen (2014). "Evidence for a weakening relationship between interannual temperature variability and northern vegetation activity." Nat Commun **5**: 5018. DOI: 10.1038/ncomms6018

Piao, S., S. Sitch, P. Ciais, P. Friedlingstein, P. Peylin, X. Wang, A. Ahlstrom, A. Anav, J. G. Canadell, N. Cong, C. Huntingford, M. Jung, S. Levis, P. E. Levy, J. Li, X. Lin, M. R. Lomas, M. Lu, Y. Luo, Y. Ma, R. B. Myneni, B. Poulter, Z. Sun, T. Wang, N. Viovy, S. Zaehle and N. Zeng (2013). "Evaluation of terrestrial carbon cycle models for their response to climate variability and to CO_2 trends." Glob Chang Biol **19**(7): 2117-2132. DOI: 10.1111/gcb.12187

Ping, C.-L., G. J. Michaelson, M. T. Jorgenson, J. M. Kimble, H. Epstein, V. E. Romanovsky and D. A. Walker (2008). "High stocks of soil organic carbon in the North American Arctic region." Nature Geosci **1**(9): 615-619. DOI: http://www.nature.com/ngeo/journal/v1/n9/suppinfo/ngeo284_S1.html

Randerson, J. T., H. Liu, M. G. Flanner, S. D. Chambers, Y. Jin, P. G. Hess, G. Pfister, M. C. Mack, K. K. Treseder, L. R. Welp, F. S. Chapin, J. W. Harden, M. L. Goulden, E. Lyons, J. C. Neff, E. A. G. Schuur and C. S. Zender (2006). "Impact of boreal forest fire on climate warming." Science **314**: 1130 - 1132.

Rocha, A. V. and G. R. Shaver (2011). "Burn severity influences postfire CO_2 exchange in arctic tundra." Ecological Applications **21**(2): 477-489.

Rogers, A. (2014). "The use and misuse of V(c,max) in Earth System Models." Photosynth Res **119**(1-2): 15-29. DOI: 10.1007/s11120-013-9818-1

Rogers, A., S. P. Serbin, K. S. Ely, V. L. Sloan and S. D. Wullschleger (2017). "Terrestrial biosphere models underestimate photosynthetic capacity and CO2 assimilation in the Arctic." New Phytol. DOI: 10.1111/nph.14740

Running, W. S., R. R. Nemani, F. A. Heinsch, M. Zhao, Reeves M and H. Hashimoto (2004). "A continuous satellite-derived measure of global terrestrial primary production." BioScience **54**(6): 547-560.

Ryu, Y., D. D. Baldocchi, T. A. Black, M. Detto, B. E. Law, R. Leuning, A. Miyata, M. Reichstein, R. Vargas, C. Ammann, J. Beringer, L. B. Flanagan, L. Gu, L. B. Hutley, J. Kim, H. McCaughey, E. J. Moors, S. Rambal and T. Vesala (2012). "On the temporal upscaling of evapotranspiration from instantaneous remote sensing measurements to 8-day mean daily-sums." Agricultural and Forest Meteorology **152**: 212-222. DOI: 10.1016/j.agrformet.2011.09.010

Ryu, Y., D. D. Baldocchi, H. Kobayashi, C. van Ingen, J. Li, T. A. Black, J. Beringer, E. van Gorsel, A. Knohl, B. E. Law and O. Roupsard (2011). "Integration of MODIS land and atmosphere products with a coupled-process model to estimate gross primary productivity and evapotranspiration from 1 km to global scales." Global Biogeochemical Cycles **25**(4). DOI: http://dx.doi.org/10.1029/2011gb004053

Ryu, Y., C. Jiang, H. Kobayashi and M. Detto (2018). "MODIS-derived global land products of shortwave radiation and diffuse and total photosynthetically active radiation at 5 km resolution from 2000." Remote Sensing of Environment. DOI: 10.1016/j.rse.2017.09.021

Schuur, E. A., A. D. McGuire, C. Schadel, G. Grosse, J. W. Harden, D. J. Hayes, G. Hugelius, C. D. Koven, P. Kuhry, D. M. Lawrence, S. M. Natali, D. Olefeldt, V. E. Romanovsky, K. Schaefer, M. R. Turetsky, C. C. Treat and J. E. Vonk (2015). "Climate change and the permafrost carbon feedback." Nature **520**(7546): 171-179. DOI: 10.1038/nature14338

Schwalm, C., R.,, T. A. Black, B. D. Amiro, M. A. Arain, A. G. Barr, C. P. A. Bourque, A. L. Dunn, K. B. Flanagan, M. Giasson, P. M. Lafleur, H. A. Margolis, J. H. McCaughey, A. L. Orchansky and S. C. Wofsy (2006). "Photosynthetic light use efficiency of three biomes across an east–west continental-scale transect in Canada." Agricultural and Forest Meteorology **140**(1-4): 269-286. DOI: 10.1016/j.agrformet.2006.06.010

Seddon, A. W., M. Macias-Fauria, P. R. Long, D. Benz and K. J. Willis (2016). "Sensitivity of global terrestrial ecosystems to climate variability." Nature **531**(7593): 229-232. DOI: 10.1038/nature16986

Shaver, G. R., L. E. Street, E. B. Rastetter, M. T. Van Wijk and M. Williams (2007). "Functional convergence in regulation of net CO_2 flux in heterogeneous tundra landscapes in Alaska and Sweden." Journal of Ecology **95**(4): 802-817. DOI: 10.1111/j.1365-2745.2007.01259.x

Sitch, S., A. D. McGuire, J. S. Kimball and K. Mcdonald (2007). "Assessing the Carbon Balance of Circumpolar Arctic Tundra Using remote sensing and process modeling." Ecological Applications **17**(1): 213-234.

Sjöström, M., M. Zhao, S. Archibald, A. Arneth, B. Cappelaere, U. Falk, A. de Grandcourt, N. Hanan, L. Kergoat, W. Kutsch, L. Merbold, E. Mougin, A. Nickless, Y. Nouvellon, R. J. Scholes, E. M. Veenendaal and J. Ardö (2013). "Evaluation of MODIS gross primary productivity for Africa using eddy covariance data." Remote Sensing of Environment **131**: 275-286. DOI: 10.1016/j.rse.2012.12.023

Strauss, J., L. Schirrmeister, G. Grosse, S. Wetterich, M. Ulrich, U. Herzschuh and H. W. Hubberten (2013). "The deep permafrost carbon pool of the Yedoma region in Siberia and Alaska." Geophys Res Lett **40**(23): 6165-6170. DOI: 10.1002/2013GL058088

Thompson, C., J. Beringer, F. S. Chapin, III and A. D. McGuire (2004). "Structural complexity and land surface energy exchange along a gradient from arctic tundra to boreal forest." Journal of Vegetation Science **15**: 397-406.

Tramontana, G., M. Jung, C. R. Schwalm, K. Ichii, G. Camps-Valls, B. Ráduly, M. Reichstein, M. A. Arain, A. Cescatti, G. Kiely, L. Merbold, P. Serrano-Ortiz, S. Sickert, S. Wolf and D. Papale (2016). "Predicting carbon dioxide and energy fluxes across global FLUXNET sites with regression algorithms." Biogeosciences **13**(14): 4291-4313. DOI: 10.5194/bg-13-4291-2016

Turner, D. P., W. D. Ritts, W. B. Cohen, S. T. Gower, S. W. Running, M. Zhao, M. H. Costa, A. A. Kirschbaum, J. M. Ham, S. R. Saleska and D. E. Ahl (2006). "Evaluation of MODIS NPP and GPP products across multiple biomes." Remote Sensing of Environment **102**(3-4): 282-292. DOI: 10.1016/j.rse.2006.02.017

Ueyama, M., Y. Harazono, E. Ohtaki and A. Miyata (2006). "Controlling factors on the interannual CO2 budget at a subarctic black spruce forest in interior Alaska." Tellus B: Chemical and Physical Meteorology **58**(5): 491-501. DOI: 10.1111/j.1600-0889.2006.00205.x

Ueyama, M., K. Ichii, H. Iwata, E. S. Euskirchen, D. Zona, A. V. Rocha, Y. Harazono, C. Iwama, T. Nakai and W. C. Oechel (2013). "Upscaling terrestrial carbon dioxide fluxes in Alaska with satellite remote sensing and support vector regression." Journal of Geophysical Research: Biogeosciences **118**(3): 1266-1281. DOI: 10.1002/jgrg.20095

Ueyama, M., K. Ichii, H. Iwata, E. S. Euskirchen, D. Zona, A. V. Rocha, Y. Harazono, C. Iwama, T. Nakai and W. C. Oechel (2014). "Change in surface energy balance in Alaska due to fire and spring warming, based on upscaling eddy covariance measurements." Journal of Geophysical Research: Biogeosciences **119**(10): 1947-1969. DOI: 10.1002/2014jg002717

Ueyama, M., H. Iwata and Y. Harazono (2014). "Autumn warming reduces the CO2 sink of a black spruce forest in interior Alaska based on a nine-year eddy covariance measurement." Glob Chang Biol **20**(4): 1161-1173. DOI: 10.1111/gcb.12434

Ueyama, M., H. Iwata, Y. Harazono, E. S. Euskirchen., W. C. Oechel. and D. Zona (2013). "Growing season and spatial variations of carbon fluxes of Arctic and boreal ecosystems of Alaska." Ecological Applications **23**(8): 1798-1816.

Walker, A. P., A. P. Beckerman, L. Gu, J. Kattge, L. A. Cernusak, T. F. Domingues, J. C. Scales, G. Wohlfahrt, S. D. Wullschleger and F. I. Woodward (2014). "The relationship of leaf photosynthetic traits - V cmax and J max - to leaf nitrogen, leaf phosphorus, and specific leaf area: a meta-analysis and modeling study." Ecol Evol **4**(16): 3218-3235. DOI: 10.1002/ece3.1173

Walker, D. A., M. K. Raynolds, F. J. A. Daniëls, E. Einarsson, A. Elvebakk, W. A. Gould, A. E. Katenin, S. S. Kholod, C. J. Markon, E. S. Melnikov, N. G. Moskalenko, S. S. Talbot, B. A. Yurtsev and t. o. m. o. t. C. Team (2005). "The Circumpolar Arctic Vegetation map." Journal of Vegetation Science **16**: 267 - 282.

Wang, L., H. Zhu, A. Lin, L. Zou, W. Qin and Q. Du (2017). "Evaluation of the Latest MODIS GPP Products across Multiple Biomes Using Global Eddy Covariance Flux Data." Remote Sensing **9**(5): 418. DOI: 10.3390/rs9050418

Wang, X., S. Piao, X. Xu, P. Ciais, N. MacBean, R. B. Myneni and L. Li (2015). "Has the advancing onset of spring vegetation green-up slowed down or changed abruptly over the last three decades?" Global Ecology and Biogeography **24**(6): 621-631. DOI: 10.1111/geb.12289

Welp, L. R., J. T. Randerson and H. P. Liu (2007). "The sensitivity of carbon fluxes to spring warming and summer drought depends on plant functional type in boreal forest ecosystems." Agricultural and Forest Meteorology **147**(3-4): 172-185. DOI: 10.1016/j.agrformet.2007.07.010

Williams, M., L. E. Street, M. T. van Wijk and G. R. Shaver (2006). "Identifying Differences in Carbon Exchange among Arctic Ecosystem Types." Ecosystems **9**(2): 288-304. DOI: 10.1007/s10021-005-0146-y

Xu, L., R. B. Myneni, F. S. Chapin Iii, T. V. Callaghan, J. E. Pinzon, C. J. Tucker, Z. Zhu, J. Bi, P. Ciais, H. Tømmervik, E. S. Euskirchen, B. C. Forbes, S. L. Piao, B. T. Anderson, S. Ganguly, R. R. Nemani, S. J. Goetz, P. S. A. Beck, A. G. Bunn, C. Cao and J. C. Stroeve (2013). "Temperature and vegetation seasonality diminishment over northern lands." Nature Climate Change. DOI: 10.1038/nclimate1836

Yi, Y., J. S. Kimball, L. A. Jones, R. H. Reichle, R. Nemani and H. A. Margolis (2013). "Recent

climate and fire disturbance impacts on boreal and arctic ecosystem productivity estimated using a satellite-based terrestrial carbon flux model." Journal of Geophysical Research: Biogeosciences **118**(2): 606-622. DOI: 10.1002/jgrg.20053

Yuan, W., Y. Luo, A. D. Richardson, R. A. M. Oren, S. Luyssaert, I. A. Janssens, R. Ceulemans, X. Zhou, T. GrÜNwald, M. Aubinet, C. Berhofer, D. D. Baldocchi, J. Chen, A. L. Dunn, J. L. Deforest, D. Dragoni, A. H. Goldstein, E. Moors, J. William Munger, R. K. Monson, A. E. Suyker, G. Starr, R. L. Scott, J. Tenhunen, S. B. Verma, T. Vesala and S. C. Wofsy (2009). "Latitudinal patterns of magnitude and interannual variability in net ecosystem exchange regulated by biological and environmental variables." Global Change Biology **15**(12): 2905-2920. DOI: 10.1111/j.1365-2486.2009.01870.x

Zeng, Z., S. Piao, L. Z. X. Li, L. Zhou, P. Ciais, T. Wang, Y. Li, X. Lian, E. F. Wood, P. Friedlingstein, J. Mao, L. D. Estes, Ranga B. Myneni, S. Peng, X. Shi, S. I. Seneviratne and Y. Wang (2017). "Climate mitigation from vegetation biophysical feedbacks during the past three decades." Nature Climate Change **7**(6): 432-436. DOI: 10.1038/nclimate3299

Zhang, Y., X. Xiao, L. Guanter, S. Zhou, P. Ciais, J. Joiner, S. Sitch, X. Wu, J. Nabel, J. Dong, E. Kato, A. K. Jain, A. Wiltshire and B. D. Stocker (2016). "Precipitation and carbon-water coupling jointly control the interannual variability of global land gross primary production." Sci Rep **6**: 39748. DOI: 10.1038/srep39748

Zhang, Z., R. Zhang, A. Cescatti, G. Wohlfahrt, N. Buchmann, J. Zhu, G. Chen, F. Moyano, J. Pumpanen, T. Hirano, K. Takagi and L. Merbold (2017). "Effect of climate warming on the annual terrestrial net ecosystem CO2 exchange globally in the boreal and temperate regions." Sci Rep **7**(1): 3108. DOI: 10.1038/s41598-017-03386-5

Zhao, M., S. W. Running and R. R. Nemani (2006). "Sensitivity of Moderate Resolution Imaging Spectroradiometer (MODIS) terrestrial primary production to the accuracy of meteorological reanalyses." Journal of Geophysical Research **111**(G1). DOI: 10.1029/2004jg000004

Zhou, S., Y. Zhang, P. Ciais, X. Xiao, Y. Luo, K. K. Caylor, Y. Huang and G. Wang (2017). "Dominant role of plant physiology in trend and variability of gross primary productivity in North America." Sci Rep **7**: 41366. DOI: 10.1038/srep41366

Zona, D., D. A. Lipson, K. T. Paw U, S. F. Oberbauer, P. Olivas, B. Gioli and W. C. Oechel (2012). "Increased CO_2 loss from vegetated drained lake tundra ecosystems due to flooding." Global Biogeochemical Cycles **26**(2): n/a-n/a. DOI: 10.1029/2011gb004037

Zona, D., D. A. Lipson, R. C. Zulueta, S. F. Oberbauer and W. C. Oechel (2011). "Microtopographic controls on ecosystem functioning in the Arctic Coastal Plain." Journal of Geophysical Research **116**. DOI: 10.1029/2009jg001241

Abstract in Korean

초록

이제인
서울대학교 농업생명과학대학원
협동과정 농림기상학

고 위도 생태계에 존재하는 식생은 기후 인자에 의해 즉각 적으로 변화하며, 년간 총 1차 생산성 (GPP)의 년간 변동을 초래한다. 그러므로, GPP의 시공간적 패턴 및 기후 인자가 GPP의 연간 변화 (IAV)에 어떤 영향을 주는 지를 이해하는 것은 현재와 미래의 상태를 설명하는데 중요하다. 본 연구에서는 알래스카지역의 GPP 시공간적 패턴을 검토하고 기후 인자와의 연관성을 밝혔다. 우리는 GPP를 서로 다른 4개의 접근 방법 모델들, a process-based (Breathing Earth System Simulator), a semi-empirical (Moderate Resolution Spectroradiometer 17A2) and the machine-learning (Support Vector Regression and FLUXCOM)을 사용하였다. 17개의 알래스카 지역에서 얻은 에디 공분산 자료를 이용하여 모델들을 평가한 결과, 65%에서 85%의 월별 변화를 보였으며, -22%에서 33%까지의 상대적 편차를 나타내었고, 북쪽 수림대에서 툰드라지역과 불에 훼손된 지역보다 더 좋은 모델 성능을 보였다. 모든 모델로부터 얻은 GPP의 시공간 분포는 낙엽 활엽수림에서 상대적으로 가장 큰 년간 변화 기여도 (14%)를, 화재와 상록수림 (13%), 그리고 툰드라 (10%) 순으로 일정한 패턴을 보였다. 툰드라에서의 GPP의 IAV 비율은 55%로 가장 컸으며, 상록수림은 (38%), 낙엽 활엽수림은 (7%) 그리고 화재에 의해 훼손됐었던 지역은 (0.8%)의 결과를 보였다. 툰드라 지역의 GPP는 식생 유형 중 가장 작은 변화를 보였지만, 알래스카의 68%는 툰드라이므로 GPP의 IAV에 가장 큰 기여를 하였다. 2001년부터 2011년까지의 GPP의 IAV는 대기 온도 및 일사량의 IAV와 비슷한 패턴을 나타냈으며, 더운 해에는 추운 해에 비해 많은 량의 anomaly GPP 를 보였다. 그러므로, 기후 변화의 결과인 온도 변화는 대지와 대기 간 이산화 탄소 순환의 변화에 중요한 영향을 미칠 수 있다

주요어:. 연간 변화, 총1차 생산성, 온도, 일사량, 강수량, 알라스카
학 번 : 2015-23147.